Journal of Earth Science, *Vol. 20*, *No. 3*, *p. 546–554*, *June 2009* *ISSN 1674-487X*
Printed in China
DOI: 10.1007/s12583-009-0045-9

Applications of Engineering Seismology for Site Characterization

Oz Yilmaz*, **Murat Eser**
Anatolian Geophysical, 28 *Lalebayiri*, *Kemer Country*, *Kemerburgaz*, *Istanbul* 34077, *Turkey*
Mehmet Berilgen
Yildiz Technical University, *Istanbul*, *Turkey*

ABSTRACT: We determined the seismic model of the soil column within a residential project site in Istanbul, Turkey. Specifically, we conducted a refraction seismic survey at 20 locations using a receiver spread with 484.5-Hz vertical geophones at 2-m intervals. We applied nonlinear tomography to first-arrival times to estimate the P-wave velocity-depth profiles and performed Rayleigh-wave inversion to estimate the S-wave velocity-depth profiles down to a depth of 30 m at each of the locations. We then combined the seismic velocities with the geotechnical borehole information regarding the lithology of the soil column and determined the site-specific geotechnical earthquake engineering parameters for the site. Specifically, we computed the maximum soil amplification ratio, maximum surface-bedrock acceleration ratio, depth interval of significant acceleration, maximum soil-rock response ratio, and design spectrum periods *TA–TB*. We conducted reflection seismic surveys along five line traverses with lengths between 150 and 300 m and delineated landslide failure surfaces within the site. We recorded shot gathers at 2-m intervals along each of the seismic line traverses using a receiver spread with 4 840-Hz vertical geophones at 2-m intervals. We applied nonlinear tomography to first-arrival times to estimate a P-wave velocity-depth model and analyzed the reflected waves to obtain a seismic image of the deep near-surface along each of the line traverses.

KEY WORDS: engineering seismology, geotechnical engineering, earthquake engineering, shear-wave velocity.

INTRODUCTION

A geotechnical project involves interdisciplinary coordination among the seismologist, the geomorphologist, and the geotechnical engineer (Fig. 1). We obtain a seismic image of the near-surface from the analysis of reflected waves to delineate fault geometry and geometry of layers within the soil column. We then obtain a P-wave velocity-depth model of the soil column from the analysis of refracted waves. Finally, we estimate an S-wave velocity-depth profile for the soil column from the analysis of surface waves. The parameters associated with the soil geometry, soil pedology, and the soil dynamics constitute the geotechnical model of the soil column, which is then used for the geotechnical design for soil remediation.

Figure 2 shows the location of the site. The size of the area is approximately 40 acres. Elevations vary between 125 and 180 m. The topography is fairly flat at the western half of the site while there is a downhill slope in the northerly direction at the eastern half. The top soil is entirely clay. The site has been designated for a residential project that involves the construction of multistorey apartment blocks.

*Corresponding author: oz@anatoliangeo.com

Manuscript received October 17, 2008.
Manuscript accepted February 11, 2009.

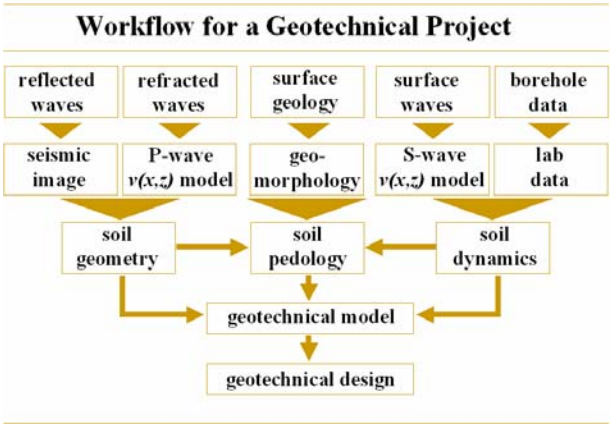

Figure 1. Workflow for a geotechnical project includes seismic surveys to delineate the soil geometry and estimate the P- and S-wave velocities of the soil column.

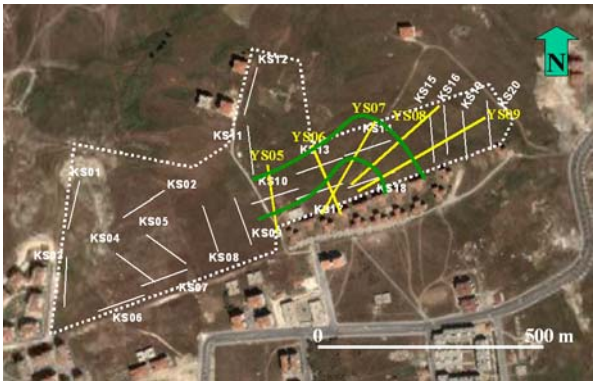

Figure 2. Location map for the seismic survey conducted within the residential development project site. The survey consisted of refraction profiling at 20 locations (KS01–20) and reflection profiling along five line traverses (YS05–09). The white lines denote the orientation of the receiver spreads for the refraction survey. The green curves denote the extremities of the landslide failure zone.

DATA ACQUISITION

At each of the 20 refraction-survey locations (KS01–KS20) within the project site (Fig. 2), we deployed a receiver spread with 484.5-Hz vertical geophones at 2-m intervals. We used a buffalo gun at the bottom of a charge hole with a diameter of 10 cm and a depth of 30 cm, and acquired three shot records with source locations at each end of the spread and at the center of the spread (Fig. 3). The sampling rate for recording was 0.5 ms and the record length was 2 s. The orientation of the receiver spread at each location

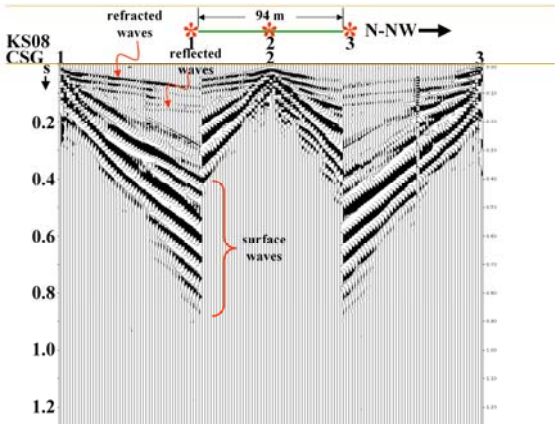

Figure 3. Example common-shot gathers acquired by a 94-m receiver spread (the green bar on top) at location KS08. The red asterisks denote the shot locations—two shots with 2-m offset from the ends of the receiver spread and a shot at the center of the spread.

was chosen such that the elevation change along the receiver spread was minimal.

Along each of the five reflection-survey lines within the project site (Fig. 2), we deployed a receiver spread with 4 840-Hz vertical geophones at 2-m intervals. We used a hand hammer and a steel plate, and acquired hundreds of shot records at 2-m intervals along each of the seismic lines with lengths between 150 and 300 m. The sampling rate for recording was 0.5 ms and the record length was 1 s.

ANALYSIS OF REFRACTED AND SURFACE WAVES

By applying a nonlinear traveltime tomography (Zhang and Toksoz, 1997) to the first-arrival times picked from the three shot records (Fig. 4), we estimated a near-surface P-wave velocity-depth model along the receiver spread at each of the 20 locations. By applying smoothing during the inversion and lateral averaging after the inversion, we then obtained a P-wave velocity-depth profile down to a depth of 30 m representative of each location.

We applied a workflow (Yilmaz and Eser, 2002) for the analysis of the first-arrival times that are primarily associated with refracted waves. First, an initial P-wave velocity-depth model was derived from the traveltimes picked from the field records. Then, this

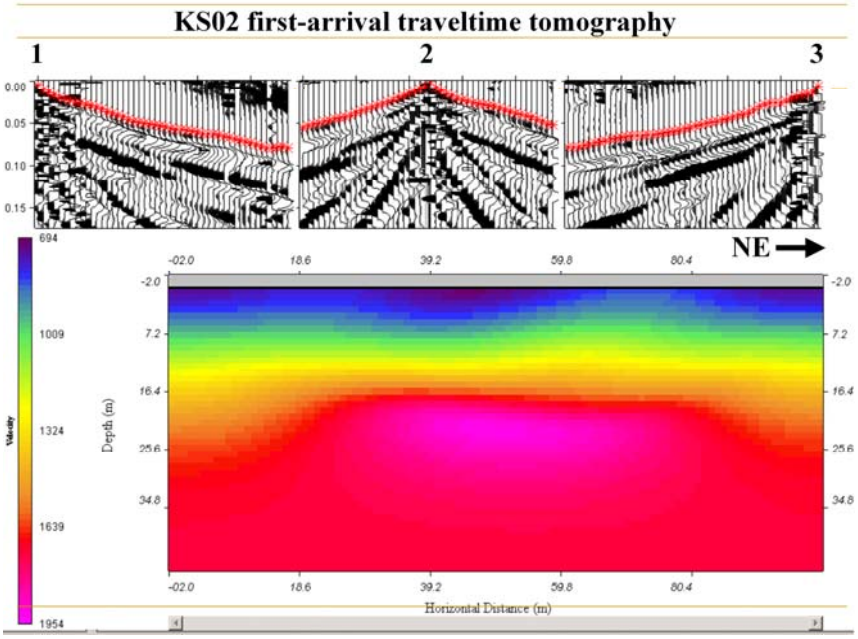

Figure 4. First-arrival times (denoted by the red asterisks) picked from three shot records at location KS02 (top), and the P-wave velocity-depth model estimated by nonlinear inversion of the traveltimes (bottom).

'initial' model was perturbed iteratively by nonlinear traveltime tomography to estimate a 'final' P-wave velocity-depth model (Fig. 4). At each iteration, first-arrival times were modeled and compared with the actual (picked) traveltimes. Iteration was stopped when the discrepancy between the modeled and actual traveltimes was reduced to an acceptable minimum.

Next, we identified at each KS location the off-end shot record with the most pronounced dispersive Rayleigh-type surface-wave pattern (Fig. 5), which was first isolated from the refracted and reflected waves by inside and outside mutes, then filtered using a 2, 4–36, 48-Hz passband to remove low- and high-frequency noise. We then performed plane-wave decomposition to transform the data from offset-time to phase-velocity versus frequency domain (Fig. 6). A dispersion curve associated with the fundamental mode of the surface waves was picked in the transform domain based on the maximum-energy criterion (Fig. 6) and inverted to estimate the S-wave velocity as a function of depth (Fig. 5; Park et al., 1999; Xia et al., 1999). In this procedure, initial depth-profiles for P- and S-wave velocities are iteratively perturbed until a final S-wave velocity-depth profile is estimated. At each iteration, modeled dispersion values and the picked (actual) dispersion values are compared.

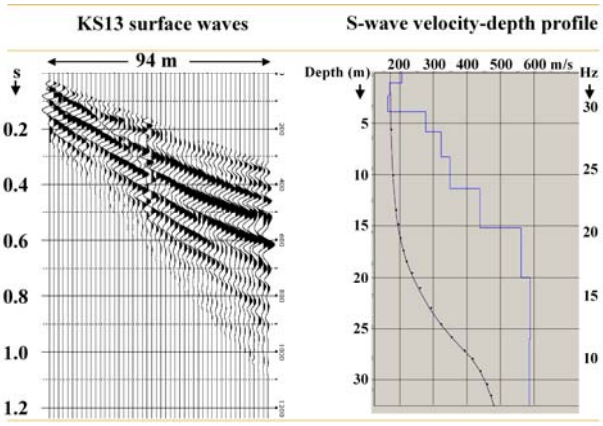

Figure 5. Dispersive surface waves isolated from the reflected and refracted waves on a shot record at one end of the receiver spread at location KS13 (left), and the S-wave velocity-depth profile (the blue curve) estimated by inversion of the surface waves (right). The vertical axis in depth is associated with the S-wave velocity and the vertical axis in frequency is associated with the dispersion curve as in Fig. 6. The S-wave velocity-depth profile was estimated by an iterative inversion of the dispersion curve for the Rayleigh-wave fundamental mode shown in Fig. 6. Iteration is stopped when the discrepancy between the modeled (the black curve on the right) and actual dispersion values (the black dots on the right) is reduced to an acceptable minimum.

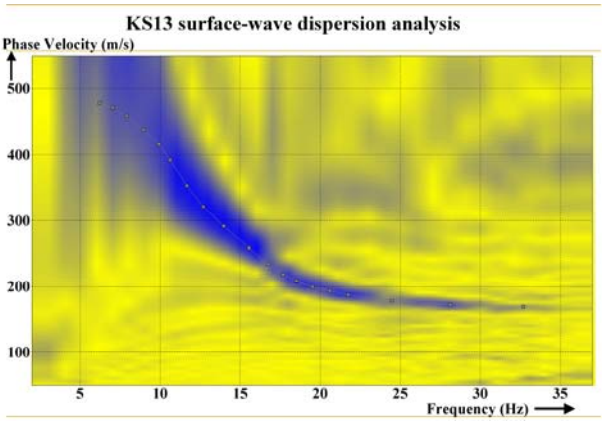

Figure 6. Dispersion spectrum of the surface waves in the shot record shown in Fig. 5, computed after the plane-wave decomposition. In this figure, the vertical axis represents the phase velocity of Rayleigh waves. Note that each frequency component of the Rayleigh waves travels at a different speed, thus the dispersive character of these waves within the soil column. The largest portion of the Rayleigh-wave energy often, but not always, is associated with the fundamental mode. For this mode, a dispersion curve that represents the change of phase velocity with frequency is picked as shown. Then, this dispersion curve is used in an inversion algorithm to estimate the S-wave velocity-depth profile for the soil column at the KS locations (Fig. 5).

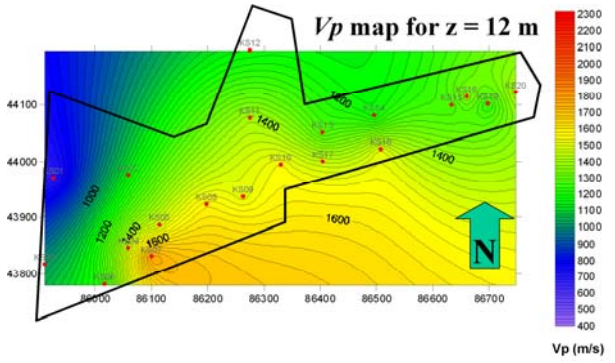

Figure 7. The P-wave velocity map for a depth level of 12 m created by three-dimensional interpolation of the P-wave velocity-depth functions associated with the 20 locations (indicated by the red dots) where the refraction seismic survey was conducted. These velocity functions were derived by lateral averaging of the P-wave velocity-depth models as in Fig. 4 at each of the KS locations. The black polygon defines the boundaries of the project site.

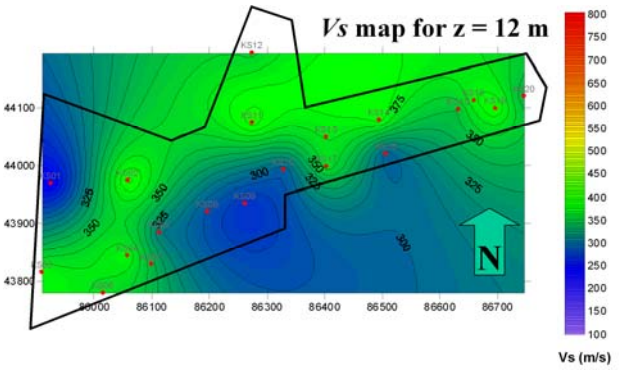

Figure 8. The S-wave velocity map for a depth level of 12 m created by three-dimensional interpolation of the S-wave velocity-depth functions as in Fig. 5 associated with the 20 locations (indicated by the red dots) where the refraction seismic survey was conducted. The black polygon defines the boundaries of the project site.

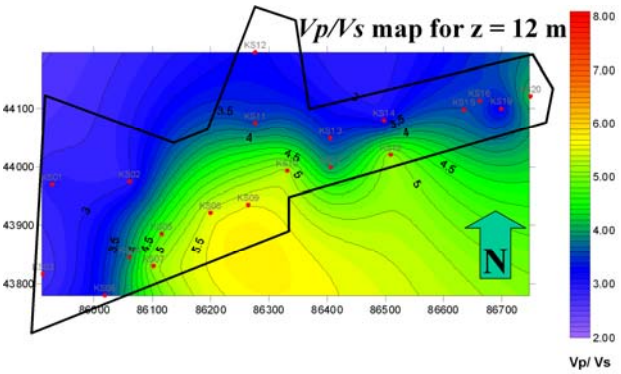

Figure 9. The P- to S-wave velocity ratio map for a depth level of 12 m created by three-dimensional interpolation of the P- and S-wave velocity-depth functions associated with the 20 locations (indicated by the red dots) where the refraction seismic survey was conducted. The P-wave velocity functions were derived by lateral averaging of the P-wave velocity-depth models as in Fig. 4 at each of the KS locations. The S-wave velocity-depth functions are as in Fig. 5. The black polygon defines the boundaries of the project site.

Iteration is stopped when the discrepancy between the modeled and actual dispersion values is reduced to an acceptable minimum. The velocity estimation from surface waves represents a lateral average over the receiver spread length in contrast with the velocity estimation from borehole seismic measurements that are influenced by localized lithologic anomalies and

borehole conditions.

Following the analysis of refracted waves to estimate the P-wave velocities and the analysis of surface waves to estimate the S-wave velocities at each of the 20 locations, we interpolated the velocities and generated velocity contour maps for depth levels of 0 to 30 m at 4-m intervals (Figs. 7 and 8). Additionally, we computed the ratio of the P-wave velocities to the S-wave velocities as a function of depth and generated the velocity-ratio contour maps (Fig. 9). Based on the velocity variations, the site was divided into three sections—the western section with relatively low S-wave velocities, the eastern section with relatively high S-wave velocities, and the transitional central section (Fig. 10). We then drilled geotechnical boreholes within each section down to a depth of 50, 40, and 30 m at locations coincident with the center of the spreads KS05, KS10, and KS14, respectively.

ESTIMATION OF GEOTECHNICAL EARTHQUAKE ENGINEERING PARAMETERS

For each section within the project site (western, central, and eastern), the S-wave velocities within the soil column combined with the borehole lithology (Fig. 11) were used to determine the geotechnical earthquake engineering parameters. We began with a rock-site SH accelerogram that describes the time history of the strong ground motion associated with the August 1999 Izmit earthquake (Yilmaz et al., 2006).

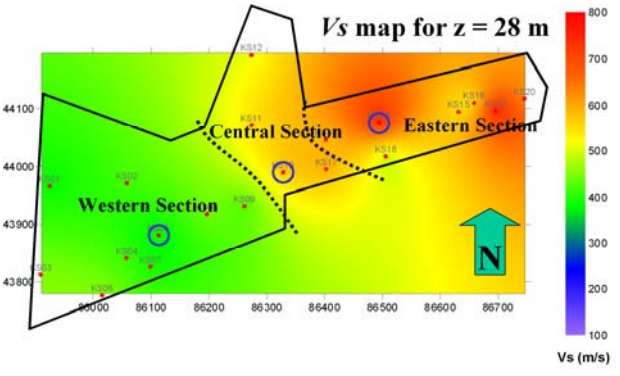

Figure 10. The S-wave velocity map for a depth level of 28 m. The red dots represent the spread centers at the 20 locations where the seismic survey was conducted. The blue circles denote the geotechnical borehole locations for each of the three sections. The black polygon defines the boundaries of the project site.

Given the S-wave velocity-depth profile, the geotechnical borehole information, and the accelerogram that describes the ground motion at the rock site, we calculated the accelerogram that simulates the ground motion at the soil site (Fig. 12) for each of the three sections within the site. This one-dimensional site-response analysis was performed using a frequency-domain algorithm that models the nonlinear material behavior of the soil column as an equivalent linear system (Bardet et al., 2000; Schnabel et al., 1972).

In earthquake engineering, the soil response to an earthquake motion is calculated based on the scenario that corresponds to a maximum possible peak ground acceleration that may occur at a location (Kramer, 1996). Hence, the accelerogram at the rock site (equivalently, at the soil-bedrock interface) was actually upscaled to a maximum value of 0.3 g before the modeling of the accelerogram at the soil sites within each section (KS05, KS10, and KS14).

From Fig. 12a, we determined for each section the ratio of the maximum ground acceleration at the soil site to the maximum acceleration at the soil-bedrock interface—often referred to as the maximum surface-bedrock acceleration ratio. For each section, we also computed the maximum acceleration as a function of depth, and determined the depth range for which the surface-bedrock acceleration ratio is significant (Fig. 13a). Specifically, as the bedrock motion is upward propagated through the soil column, maximum acceleration values are extracted from the

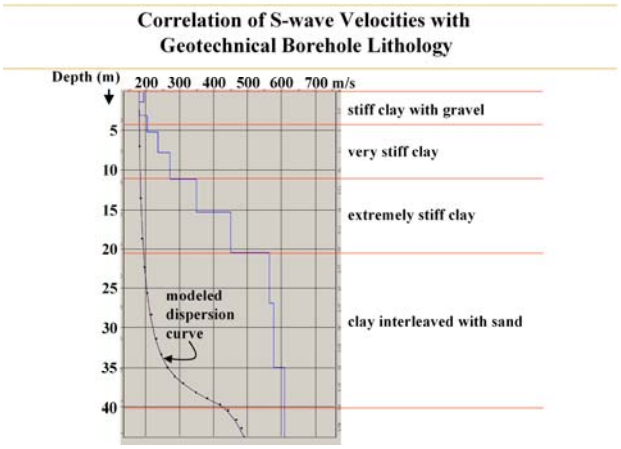

Figure 11. Correlation of the S-wave velocities with the lithology column from the geotechnical borehole at the center of the spread at location KS10 (central section in Fig. 10).

accelerograms computed at each of the discrete depth levels (Bardet et al., 2000) to obtain the curve shown in Fig. 13a. Next, we calculated the smoothed ratio of the amplitude spectra of the measured and modeled accelerograms (Fig. 12b) as shown in Fig. 13b, and determined the peak spectral amplitude at the soil site and the frequency at which this peak occurs (3.3 Hz). The latter is called the natural frequency of the soil column and the period that corresponds to the peak-amplitude frequency is called the natural period of the soil column (0.3 s). Also from Fig. 13b, we computed the ratio of the peak spectral amplitude at the soil site to the spectral amplitude corresponding to the same frequency at the rock site (2.9). This is called the maximum soil amplification ratio, which is a measure of how much the soil column amplifies the earthquake motion that occurs at the soil-bedrock interface.

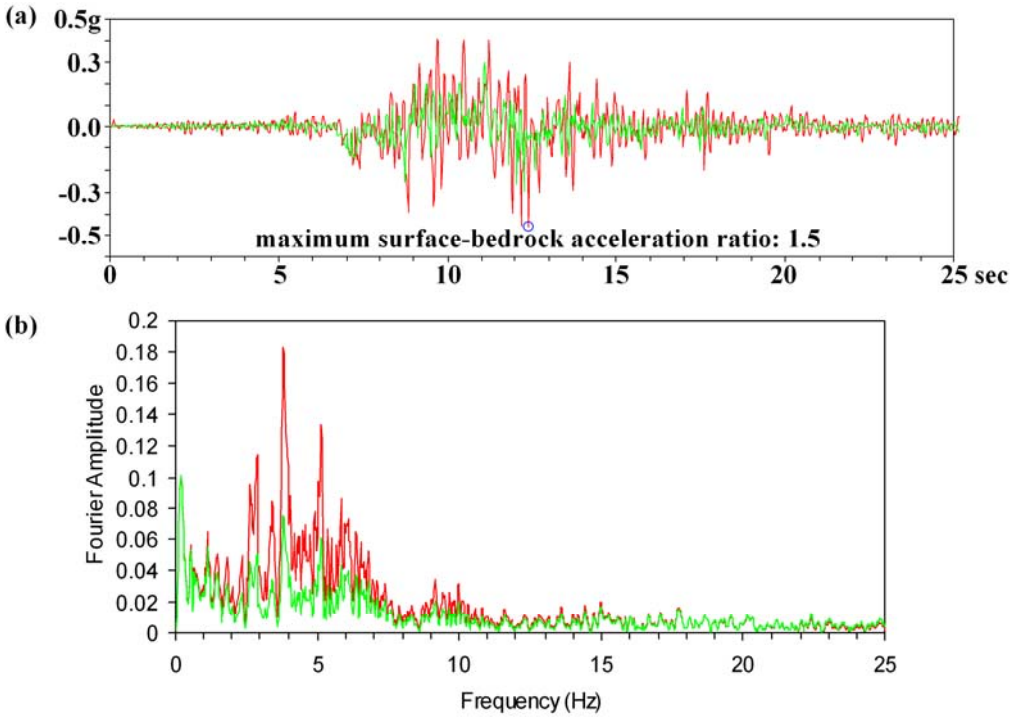

Figure 12. Analysis for geotechnical earthquake engineering parameters at site KS10 (central section in Fig. 10). (a) The accelerogram that describes the bedrock motion associated with the August 1999 Izmit earthquake measured at the rock site (green), which is assumed to be equivalent to the response at the soil-bedrock interface at the soil site (upscaled to a maximum acceleration value of 0.3 g), and the accelerogram that describes the ground motion at the soil site KS10 within the central section (red) modeled by using the velocity and borehole information given by Fig. 11. The maximum surface-bedrock acceleration ratio is 1.5. (b) The amplitude spectra of the measured and modeled accelerograms. Note that the significant amplification within soil column occurs between 0 and 12 Hz bandwidth.

Next, for each section within the site, we computed the response spectra (Fig. 13c) that describe the response of structures (buildings) with a range of natural periods to the modeled ground motion at the soil site and the actual ground motion at the rock site. The structure is defined as a spring system with a single degree of freedom, usually with a damping ratio of 5%. From Fig. 13c, we determined the maxima of the response spectra at the ground level (8 g) and soil-bedrock interface (3 g), and computed the maximum soil-rock response as the spectral acceleration ratio (2.4). We also determined the design spectrum periods *TA–TB* (0.05–0.55 s). *TA* and *TB* correspond to the minimum and maximum periods for which the spectrum is nearly flat. Outside the *TA–TB* bandwidth, the spectrum ramps down rapidly.

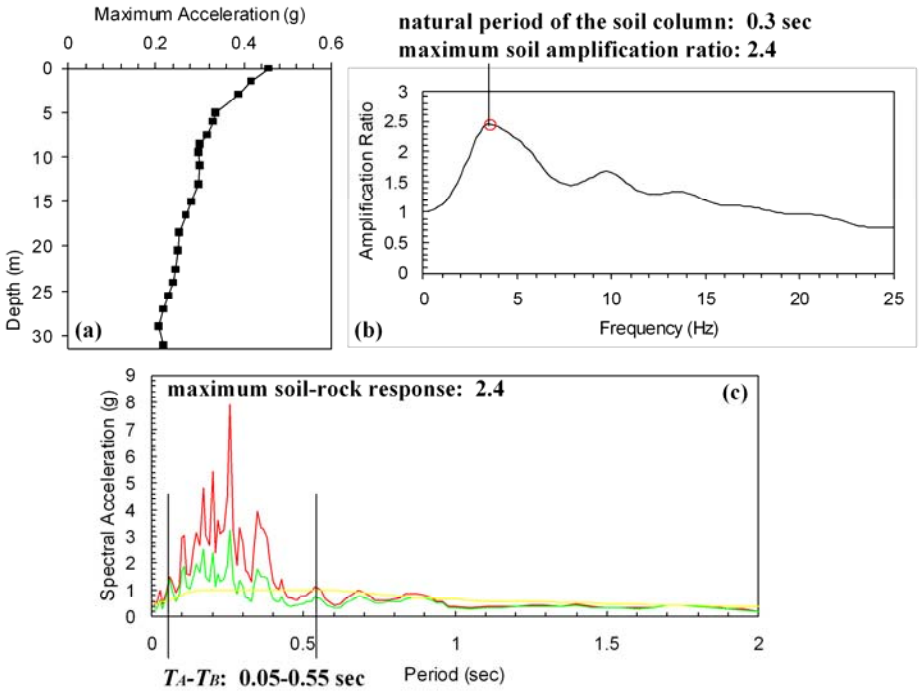

Figure 13. Analysis for geotechnical earthquake engineering parameters at site KS10 (central section in Fig. 10). (a) Maximum acceleration as a function of depth; (b) soil-bedrock amplification ratio; and (c) site-specific design spectra for the rock site (green) and the soil site (red), and the code-specific design spectrum for the soil site (yellow). Note that the most significant acceleration values at the rock site occur in *TA–TB*: 0.05–0.55 s.

Table 1 Geotechnical earthquake engineering parameters

Section	Maximum soil amplification ratio	Natural period of the soil column (s)	Maximum surface-bedrock acceleration ratio	Depth interval with significant acceleration (m)	Maximum soil-rock response	Design spectrum periods *TA–TB* (sec)
Western	2.2	0.4	1.3	0–10	1.3	0.05–0.60
Central	2.4	0.3	1.5	0–15	2.4	0.05–0.55
Eastern	2.8	0.15	1.7	0–10	2.1	0.05–0.65

Listed in Table 1 are the geotechnical earthquake engineering parameters for each of the three sections within the site. Combined with the parameters for the soil dynamics, such as the bearing capacity, these parameters are used by the geotechnical engineer for soil classification and by the civil engineer for structural design of buildings.

ANALYSIS OF REFLECTED WAVES

In contrast to a comprehensive processing sequence applied to reflection seismic data used in exploration for oil and gas fields (Yilmaz, 2001), shallow reflection seismic data usually require a simple processing sequence (Steeples and Miller, 1990) that includes application of deconvolution, time-variant spectral whitening, bandpass filtering, and automatic gain control. Aside from deriving a seismic section that represents the subsurface image down a depth of 150 m (Fig. 14), we also estimated the near-surface P-wave velocity-depth model, again using the nonlinear traveltime tomography, for each of the five line traverses (Fig. 15). The nonlinear tomography solution is based on not just the first-arrival times but also changes in traveltime gradient. As such, within the near-surface, we were able to resolve strong lateral velocity variations associated with the landslide failure surfaces (Fig. 15).

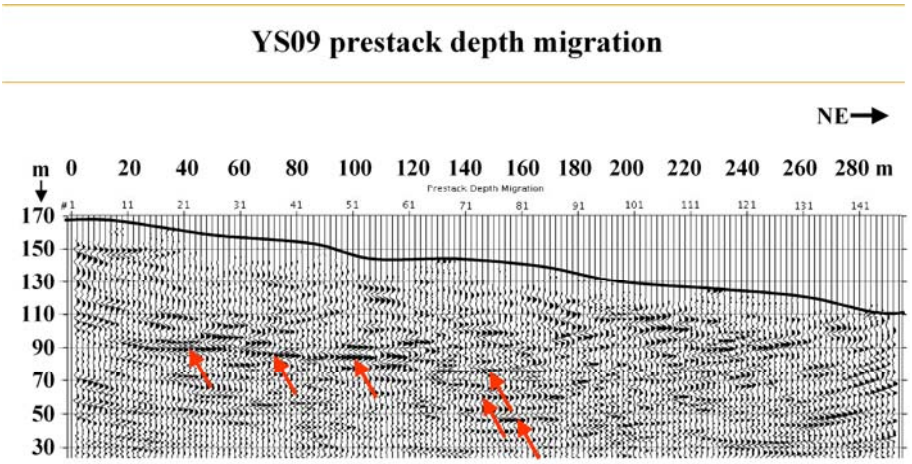

Figure 14. The seismic image of the deep near-surface along the YS09 line traverse (line location shown in Fig. 2). This image was derived by analysis of reflected waves in the shot gathers recorded along the line traverse at 2-m intervals using a receiver spread with 4 840-Hz vertical geophones. The black curve denotes approximately the topography along the line traverse. The high-amplitude reflectors indicated by the red arrows correspond to the sandstone interbeddings within the predominantly clayey soil column.

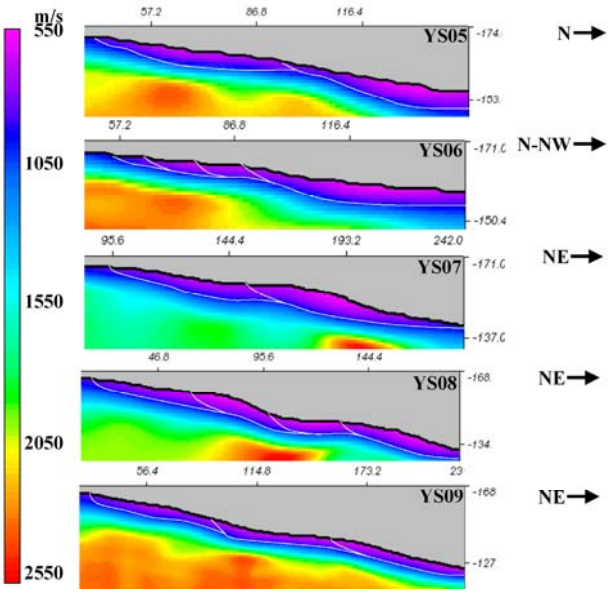

Figure 15. The P-wave velocity-depth models along the YS line traverses (line locations shown in Fig. 2). The pink zones are associated with the low-velocity landslide masses. The white curves denote the potential landslide failure surfaces.

The seismic images along the YS line traverses exhibit horizontal, piecewise continuous, but strong reflectors that are associated with sandstone interbeddings within the otherwise predominantly clayey soil column (Fig. 14), whereas the P-wave velocity-depth models along the YS line traverses exhibit low-velocity near-surface layers (Fig. 15), which, following the subsequent geotechnical borehole investigations, have been confirmed as landslide masses that are widespread within the project site (Fig. 2). Several landslide failure surfaces have been delineated as shown in Fig. 15.

CONCLUSIONS

Site investigations require multidisciplinary participation by the geologist, the seismologist, and the geotechnical and earthquake engineers. The contribution of the seismologist includes a seismic image of the near-surface from the analysis of reflected waves to delineate fault geometry and geometry of layers within the soil column, a P-wave velocity-depth model of the soil column from the analysis of refracted waves, and an S-wave velocity-depth profile for the soil column from the analysis of surface waves. As such, the role of the seismologist is to provide these intermediate products to the geotechnical engineer and earthquake engineer so as to define the parameters associated with the soil geometry, soil pedology, and the soil dynamics which constitute the geotechnical model of the soil column. In this case study, we demonstrated the role of the seismic method in defining the geotechnical model of the soil column, which can then be used for geotechnical design for soil remediation.

ACKNOWLEDGMENTS

We thank the Hanyapi Real Estate Development Corp., Istanbul, and Professor Ahmet M Işıkara for giving us the opportunity to conduct this integrated seismic project and granting the permission to publish the results.

REFERENCES CITED

Bardet, J., Ichii, K., Lin, C., 2000. Manual of EERA: A Computer Program for Equivalent-Linear Earthquake Site Response Analysis of Layered Soil Deposits. University of Southern California, Los Angeles

Kramer, S. L., 1996. Geotechnical Earthquake Engineering. Prentice-Hall, New Jersey. 273

Park, C. B., Miller, R. D., Xia, J., 1999. Multichannel Analysis of Surface Waves. *Geophysics*, 64: 800–808

Schnabel, P. B., Lysmer, P. B., Seed, H. B., 1972. SHAKE: A Computer Program for Earthquake Response Analysis of Horizontally Layered Sites. In: Report EERC 72-12, Earthquake Engineering Research Center. University of California, Berkeley

Steeples, D. W., Miller, R. D., 1990. Seismic Reflection Methods Applied to Engineering, Environmental, and Groundwater Problems. In: Ward, S. H., ed., Geotechnical and Environmental Geophysics. Soc. of Expl. Geophys., Tulsa, OK. 1–30

Xia, J., Miller, R. D., Park, C. B., 1999. Estimation of Near-Surface Shear-Wave Velocity by Inversion of Rayleigh Waves. *Geophysics*, 64: 691–700

Yilmaz, O., 2001. Seismic Data Analysis—Processing, Inversion, and Interpretation of Seismic Data. Soc. of Expl. Geophys., Tulsa, OK

Yilmaz, O., Eser, M., 2002. A Unified Workflow for Engineering Seismology. Expanded Abstracts, 72nd Annual International Meeting of the Society of Exploration Seismologists, Houston, TX

Yilmaz, O., Eser, M., Berilgen, M. M., 2006. A Case Study for Seismic Zonation in Municipal Areas. *The Leading Edge*, 25(3): 319–330

Zhang, J., Toksoz, M. N., 1997. Nonlinear Refraction Traveltime Tomography. *Geophysics*, 63: 1726–1737